European Journal of Technique

journal homepage: https://dergipark.org.tr/en/pub/ejt

Vol.12, No.2, 2022

Power Quality Analysis for Power Led Drives

Secil Genc [1], Okan Ozgonenel [2], Orkut Onat Yildiz [3] and İbrahim Hakki Kilic [3]

[1*]Ondokuz Mayis University, Electrical and Electronic Engineering Department, 55200, Samsun, Istanbul, Turkiye. (e-mail: secil.yilmaz@omu.edu.tr).
[2] Ondokuz Mayis University, Electrical and Electronic Engineering Department, 55200, Samsun, Istanbul, Turkiye. (e-mail: okanoz@omu.edu.tr).
[3]BORSAN, OSB Organize Sanayi Boulvard, Samsun, Tekkeköy, Samsun, Turkiye. (e-mail: orkutonatyildiz@borsan.com.tr).
[4] BORSAN, OSB Organize Sanayi Boulvard, Samsun, Tekkeköy, Samsun, Turkiye. (e-mail: ibrahimkilic@borsan.com.tr).

ARTICLE INFO

Received: Dec., 08. 2022
Revised: Dec., 22. 2022
Accepted: Dec, 23. 2022

Keywords:
Power quality
EMI
Conducted emissions
Harmonics

Corresponding author: *Okan Ozgonenel*

ISSN: *2536-5010* | e-ISSN: *2536-5134*

DOI: https://doi.org/10.36222/ejt.1216165

ABSTRACT

DC micro grids have grown increasingly popular in the energy grid in recent years, as distributed generation has increased. Distributed generation refers to small or large-scale renewable energy that is linked to the main power system. Renewable energy sources like solar and wind power help the local grid, but their output is inherently intermittent and unpredictable, interfering with regular grid operation. Some of these issues can be mitigated by using energy storage in conjunction with renewable energy. Renewable energy is often linked to the grid using power electronic converters.

The goal of this research is to simulate and evaluate transmitted emissions in the time and frequency planes using IEEE 1459 to investigate the impacts of DC / DC converters on DC lines, particularly for renewable energy generation. While there are standards and norms for frequencies up to 2 kHz and beginning at 150 kHz, the frequency range 2-150 kHz only has suggested techniques and propagation restrictions. As a result, the emission conveyed in the frequency range of 2-150 kHz is a subject that must be comprehended. The structure of the generation model, as well as the idea of power quality in electricity generating models, will be investigated using data collected through experimental and computer simulations on a medium-scale hybrid network connected to the grid. The technological advances acquired will subsequently be utilized to evaluate the power quality of various DC and AC single/three phase power systems (such as computer servers, airplanes, and so on).

1. INTRODUCTION

With the rise of distributed generation in recent years, DC microgrids have become increasingly widespread in the electrical grid. Distributed generation refers to small or large-scale renewable energy that links to the power grid. Wind energy, solar energy, geothermal energy, and biomass energy are all popular forms of renewable energy [1-6]. Photovoltaic cells generate direct voltage and current. Because the output of a solar cell varies depending on the weather, the regulation of such generation is done with the assistance of a DC-DC converter to regulate the power flow and voltage levels in microgrids. In a DC microgrid, DC-DC converters connect generation, energy storage, and loads, which are frequently externally networked via AC-DC converters.

There are several voltage levels of DC distribution lines. Power generating and diverse and distinct power sources (photovoltaic systems, micro turbines, wind farms, etc.), energy storage facilities (railways, subways, tram lines having various energy storage devices, roadside and on-board) (such as supercapacitors and batteries). They are all linked to a DC mains network of the same voltage level or, via converters, to a different voltage level. Furthermore, as renewable energy sources are integrated into the grid, interest in DC-DC and bidirectional AC-DC converters is growing. The usage of PWM-based converters is becoming more common as the utilization of renewable energy and battery technology grows. Aside from PWM-based converters, the growing usage of non-linear devices, electronic and electrical equipment such as SMPS, motors, fluorescent lights, electronic data processors, and power supply switches generates additional electromagnetic noise. This may have an impact on the system's stability. A DC microgrid's frequency range can range from extremely low (below 9 kHz) to very high (such as 9-150 kHz and 150 kHz-30 MHz) [7]. The increased use of DC-DC converters, which are frequently operated at higher switching frequencies, might result in electromagnetic interference (EMI) in the system. Above 2 kHz, these disruptions are referred to as "high frequency distortion" [8]. These conducted emissions have an impact on the AC mains side as well. The two primary implications of power quality problems on a distribution system are a power quality problem and the unfavorable impact on equipment (electrical loads) from power factor reduction induced by specific forms of harmonics. The Electrical Power Research Institute (EPRI) has suggested an end-user-centered definition of "power quality problem" as any power problem caused by voltage, current, or frequency variations that causes customer equipment to malfunction or misoperate. The emissions

produced by power converters used in distributed generation vary substantially not just along the time axis or in amplitude, but also across the frequency spectrum. All these components manifest as harmonics/high frequency interferences with varying amplitudes and consequences. These harmonics usually disrupt or destroy the operation of converters and other micro grid-connected devices [4], [9]. Currently, no limits are imposed by electrical distribution companies on transmitted radiated switching voltage sources, ballasts, or other equipment. However, it is apparent that emissions in this high frequency band have an impact on grid-connected devices [8]. Simultaneously, considering the EMI of the device at the original design phase will allow designers to meet electromagnetic compatibility at a reasonable cost before discovering it [10]. As a result, the power quality of these transmitted emissions should be investigated. While there are standards and norms for frequencies up to 2 kHz and beginning at 150 kHz, there are only suggested techniques and propagation limitations for frequencies between 2 and 150 kHz. As a result, new methods for frequencies in this range must be developed, or methods from other frequency ranges must be adapted [3]. There isn't enough research on the effect of high frequency disruptions on networks in the literature, it's been discovered. When the broadcasts are analyzed, it is discovered that there are insufficient research on the impact of transmitted emissions on the network. Ensini et al. [6] evaluated the effect of conducted emissions emanating from a single-phase DC-DC converter on the DC mains side in their study on the influence of transmitted emissions on the grid. Webling et al. [11] proposed a method for measuring the differential and differential mode transmitted emissions from switched-mode power sources. Jettanasen et al. investigated the nano-grid road lighting system's emitted emissions [4]. In general, power electronics switching topology in power electronics settings and electromagnetic waves propagating to the environment at MHz levels are stressed based on the transmitted propagation. Upper harmonic power quality issues have not been addressed since no study has been undertaken on the influence of released emissions into our country's grid. The strongest motivations for working in this sector have been the increased impacts of transmitted emissions on the grid and the absence of any limits, especially with the widespread use of electric cars, which is one of the development goals.

The behavior of DC and AC systems (microgrids, lines, inverter/converter equipment, etc.) that will serve as a model for power quality studies will be described in this project. In contrast to the literature, a full overview of single-phase and three-phase DC and AC systems will be offered. The goal of this project is to improve power quality and solve electromagnetic compatibility issues in DC-DC and DC/AC alternating grid connections, particularly with the increased usage of electric cars. Recommendations for measuring, analyzing, and mitigating high frequency conducted emissions will be made. Methods and methods for exact dispersion analysis will be developed. Separate analyses will be performed on the common and difference mode conducted emissions reflected on the network.

This project aims to interpret computer simulation findings and provide reports. By standardizing the higher frequencies, it is intended to help to the optimization of the Turkish energy grid, the reduction of losses, and the enhancement of power quality. In this regard, TEİAŞ released in 2021 the technical standards for the grid connection of electricity storage facilities, their monitoring using SCADA, and their usage as supplementary services. However, the influence of high-frequency disturbances on the grid induced by power converters employed in between is overlooked in this regulation. With this project, awareness of power quality issues emerging from conducted emissions that will emerge as a result of the battery's integration into the grid will be promoted, and ideas for the diversification of quality indices will be developed. In other words, awareness will be promoted regarding the development of additional laws and the standardization of the new EPDK regulation.

2. RELATED WORKS

The process of collecting, evaluating, and interpreting measurable electrical signal data is known as power quality monitoring. During the data acquisition step, voltage and current are continually measured during a specific process. Experts assist in the analysis and interpretation process. Intelligent systems may be built and deployed using breakthroughs in signal processing and artificial intelligence to automatically transform and interpret measurable data into meaningful information with minimum human interaction. Current and voltage sensors are used to measure both AC and DC systems (measuring transformers, etc). Although DC/AC metering configurations are not the primary goal of this proposed project, the best metering setups for the most efficient power quality study/research will be offered. Measurement errors induced by measurement devices, as well as connecting points, will be investigated in terms of the idea of DC power quality.

Khilnani et al. conducted a power quality assessment of emissions from a microgrid-based DC/DC converter at 0-2kHz steady state and transient loading situations within the scope of prior research. They used the quick Fourier transform to assess the experimental data (FFT). To assess DC power quality, they employed the low frequency sinusoidal distortion index (percent LFSD) and the amplitude probability distribution (APD) of voltage and current [2]. Ensini et al. investigated conducted emissions between 9 and 150 kHz in terms of DC power quality as measured by DFSB, ripple index, and APD. They compared LFSD and APD findings using CISPR 15, CISPR 14, EN50065, and EN50160 standards at various intervals [6]. Webling et al. [11] proposed a method for calculating emissions from switched-mode power sources. The rising usage of non-linear technologies has created 'power harmonics,' resulting in worse power quality. Electromagnetic noise is produced by electronic and electrical equipment such as SMPS, motors, fluorescent lamps, electronic data processors, and power supply switches. The emission produced by the device under test (DUT) will be determined not only by its internal source (electronics), but also by the quality of the incoming AC mains power. Mahesh et al. investigated how voltage harmonics impact the conducted propagation caused by DUT. Based on the experimental data, they concluded that the existence of voltage harmonics at the LISN input has a considerable impact on the DUT propagations [13]. Larrson et al. took measurements in an apartment by filtering the conducted emissions from a fluorescent bulb lighting system for a set amount of time. To minimize the harmonic content of the current, almost all fluorescent lights with high frequency ballasts employ active power factor correction (PFC) circuits. When the filtered signal is inspected, it is discovered that the converter with active PFC oscillates because of its failure to manage the current near to zero crossover. These oscillations have frequencies ranging from a few kilohertz to more than ten kHz. A three-dimensional linear scale based on short time

Fourier transform (STFT) analysis is utilized to better understand where the energy of this high frequency oscillating signal is focused [12]. Spadacini et al. suggested a circuit model for conducting emission analysis of all subsystems of an electric vehicle powertrain that can reflect both functional, low-frequency behaviour and high-frequency impacts (battery, inverter, motor). It is linked to the interface established in LISN CISPR 25 between the battery and the DC power bus. The "current-probe method" and the voltage approach were compared in CISPR 25. They stressed the importance of probe location in the CISPR current-probe approach when very high-frequency components of conducted emissions (over 30MHz) are present [14]. Spadacini et al. also evaluated the influence of difference mode (DM) and common mode (CM) currents delivered from the inverter in electric vehicle engines on the EMI's lithium-ion batteries. DM and CM currents can enter batteries via AC cables, DC wires, and ground, affecting battery performance. They developed a SPICE model of the power drive system as well as a test platform to assess the effect of the power drive system's EMI on lithium-ion batteries. They demonstrated in their experiments that the voltage fluctuation range of an unfiltered battery is greater than that of a filtered battery owing to DM and CM currents [15]. Mutoh et al. concentrated on the 1 MHz or higher frequency transient EMI noise of common mode currents produced during switching operations in electric vehicle drive systems. The fast Fourier transform was used to evaluate high frequency voltage and current data. Control strategies for reducing EMI sounds have been presented [16]. Shall and Kadi assessed the electric vehicle charger's emitted and conducted emissions in the frequency range of 150 kHz to 108 MHz in accordance with CISPR 25 IEC:2008 guidelines [17]. Korth et al. used a high frequency modelling technique to achieve a more exact estimate of the battery's voltage response owing to a high frequency current surge [18]. When the studies are analyzed, LISN is the first instrument utilized to filter the conducted emissions. The LISN is a low-pass filter that is connected between the AC or DC power source and the DUT and offers a port for creating a certain impedance and monitoring radio frequency (RF) noise. Simultaneously, the signals are seen using an EMI receiver/spectrum analyzer or data capture card. Furthermore, EMI receivers use frequency scanning or, at very high frequencies, an FFT-based time domain scan. The spectrum of the input signal is measured and analyzed by these EMI receivers [19-20]. The harmonic spectrum of the signals may be determined when the signal is delivered to the computer utilizing data capture cards for better analysis using different analysis methods [21-22]. While the EMI receiver is using FFT, the signal sent to the computer environment may be examined and compared using STFT, wavelet transforms, and Fourier transforms with different window functions. Because unstable signals in the 2-150 kHz frequency range shift over time owing to their nature, an analytical technique is necessary. As a result, the disturbances must be examined not only in the frequency domain, but also in the time-frequency domain. Because the measured value is voltage, it is represented in µV. This unit must be represented in logarithmic form, namely dBµV, and compared to the limitations in the standard in order for the limits in the frequency spectrum and test standards to be more understood. The standards used for emissions in the 2-150 kHz frequency range are: CISPR 11, which sets the mandatory limit for emission from high performance scientific, medical, or industrial equipment, and electrical lighting systems, which set the same emission limits as the CISPR 11 standard but are a very common source of broadband upper harmonic disturbance. CISPR 15, which also specifies emission limits for active supply converters, IEC TS 62578, which describes the operating conditions and typical characteristics of active supply converters, EN50065 general and EN50065 industrial (the latter two differ after 100 kHz) power line communication standards, and Standard EN 50160, which expresses low voltage, medium voltage, and high voltage supply characteristics, voltage events, and variations [3].

3. MEASUREMENT of CONDUCTED EMISSIONS

3.1. Simulation works

Fig. 1 depicts a flowchart for observing the propagation transmitted from a DC-DC buck converter with 48 V output voltage used in DC power systems. The simulation was performed in the MATLAB™ environment in order to compare it to the actual mechanism that will be implemented in the future. For comparison, the low frequency sinusoidal distortion index (percent LFSDI), ripple index, and amplitude probability distribution of DC voltage and current were determined. To restrict the transmitted emissions, IEC TS 62578, CISPR 11-15, EN50065, and EN 50160 standards were applied in this investigation. Because there is currently no standard for determining if LFSDI and APD levels are acceptable, the transmitted emissions were tested for variable input voltage and load. Wavelet transform and discrete wavelet transform methods with varied window functions, which are among the approaches proposed in related studies, have been tested for 2-150 kHz EMI band range.

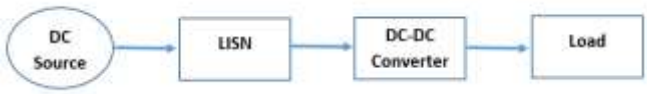

Figure 1. Flowchart of the system

MATLAB simulation circuit for power quality analysis of conducted emissions from DC-DC buck converter with varying input voltage and 48 V output voltage is given in Fig. 2. Simulation parameters are given as follows.

• Total simulation time=0.5 sec for enough the system reached steady state.

• Bandwidth: The frequency resolution has been taken as 5 ms for the collection of the signal in 200 Hz bands recommended by the EN 55065-1standard.

• Number of windows=Total time (0.5 sec)/ bandwidth (0.005 sec)=100

• Total number of samples=250000

• Number of samples in the window = Total number of samples (25000) / number of windows (100) = 2500

A time frame of 200msec is recommended by the IEC 61000-4-7 standard (5Hz frequency resolution). This scenario, however, is unsuitable for the processing of high frequency signals. As a result, the time window length for signal gathering in the 200Hz bands indicated by the EN 55065-1 standard and the standards covering frequency ranges below 150 kHz was set to 5msec.

This unit is given in logarithmic form, namely db µV, to make the restrictions in the frequency spectrum and test standards more accessible.

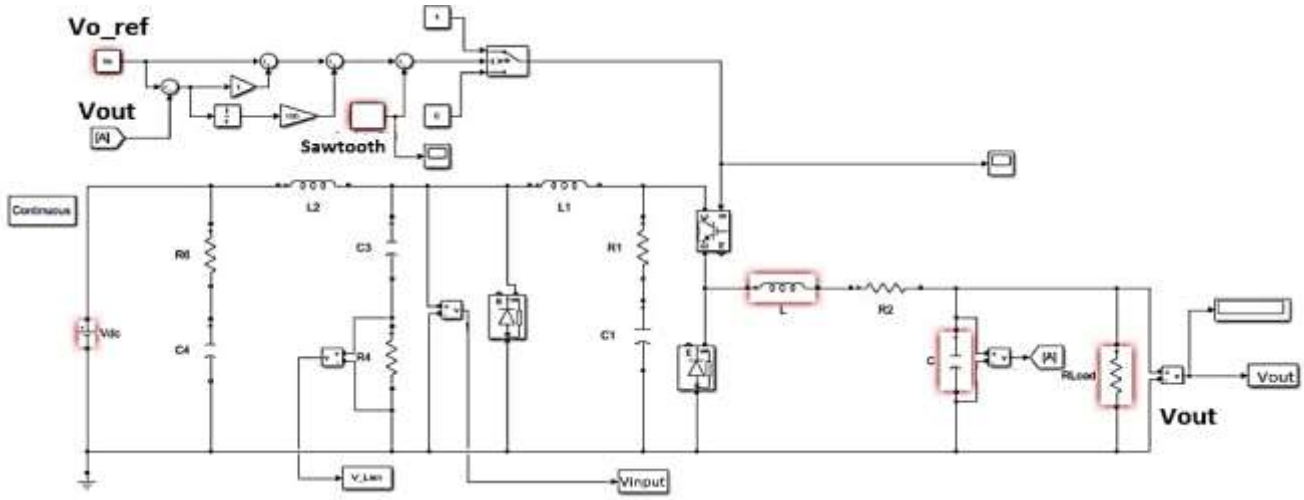

Figure 2. MATLAB simulation circuit for power quality analysis of conducted emissions from DC-DC converter

$$\mathrm{dbV} = 20\log(V) \quad (1)$$

$$db\mu V = 20\log(V) \times 10^{6} \quad (2)$$

Fig. 3 shows the input and output voltages of the DC-DC converter, as well as the voltages measured over the LISN communicated to the network side when a 2900W load is attached, when the converter input voltage is 410V and the output voltage is 48V.

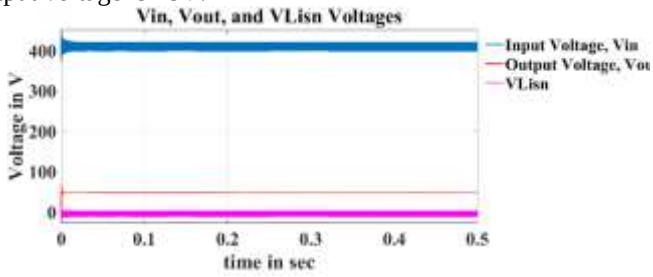

Figure 3. MATLAB simulation circuit for power quality analysis of conducted emissions from DC-DC converter

STFT analysis was done on the signal taken from the LISN output for 0.5 sec using 5msec time frames. Fig. 4 depicts the signal investigated in the 0-5msec time region. The Fourier analysis shows that, depending on the switching frequency of the converter, 20kHz and its multiples can be detected. The switching frequencies are only visible when samples are obtained above 6kHz (ignoring the transient).

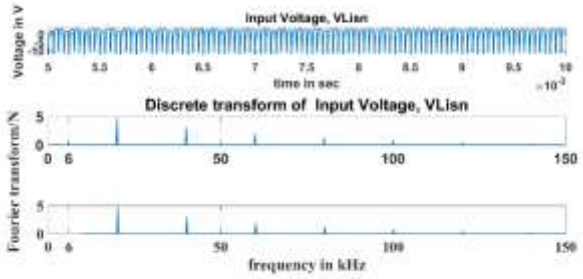

Figure 4. Amplitude variation of LISN voltage in time and frequency axis

3.2. Evaluation of conducted emission in terms of power quality indexes in DC systems

3.2.1. Distortion index

The frequency of the DC's fundamental component is zero. Instead of harmonic and internal harmonic components, Equation 3 expresses the overall effective value of low frequency sinusoidal disorder (DFSB). In Equation 3, Q[0] represents the steady-state DC value; Q[k] represents the frequency spectrum recorded for samples of q[n] over a particular time period (rms).

$$\mathrm{D} = \left[\sum_{\mathrm{k>0}}^{\mathrm{k_{max}}} (\mathrm{Q[k]/Q[0]})^2\right]^{1/2} \quad (3)$$

3.2.2. Ripple index

Equations 4,5 and 6 are used to compute the ripple index of DC-DC input voltage. Here, X_DC represents the mean DC component, X_i represents the time history sign, and X(e) represents the deviation from the mean. Due to the transient situation, samples after the first half of the 0.5sec total simulation time (after 0.25sec) were evaluated.

$$\mathrm{X_{DC}} = \frac{1}{N}\sum_{i=1}^{N} \mathrm{X_i} \quad (4)$$

$$\mathrm{X_e} = \sqrt{\frac{1}{N}\sum_{i=1}^{N} (\mathrm{X_i} - \mathrm{X_{DA}})^2} \quad (5)$$

$$\mathrm{X_e} = \frac{\mathrm{X_E}}{\mathrm{X_{DC}}} \quad (6)$$

3.2.3. Amplitude Probability Distribution (APD)

APD represents the likelihood that the interference will have a given amplitude value or more. Equation 7 calculates the APD value of the LISN output voltage. APD is the amplitude probability distribution, and FR(r) is the additive distribution function.

$$\mathrm{X_{DC}} = \frac{1}{N}\sum_{i=1}^{N} \mathrm{X_i} \quad (7)$$

4. INTRODUCTION EVALUATION of RESULTS for DC-DC BUCK CONVERTER

In simulation studies, samples obtained for 0.5sec in the simulation were evaluated by scrolling through 5msec frames. The signal's assessment in the 5-10msec time frame is shown in Figs. 5 and 6. Fig. 5, shows CE under varying load conditions. According to the result, for this window length CE exceeds the limit for EN50065 standard and increase with the load. The APD analysis depicts the probable magnitude increase from the steady state for DC voltage. As seen in Fig. 6, APD also increases with the load.

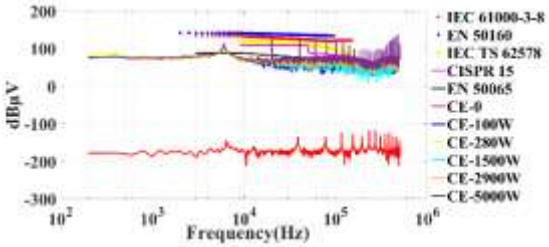

Figure 5. Variation of conducted emissions depending on load in case of 5-10msec window length, 410V input voltage

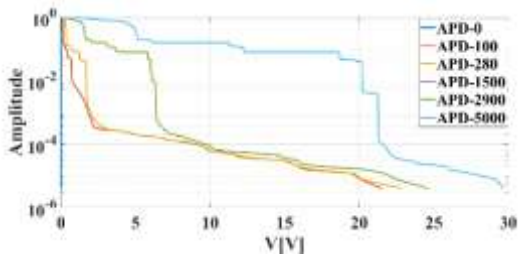

Figure 6. Change of APD depending on load in case of 5-10msec window length, 410V input voltage

Table 1. 5-10 ms Window interval, LFSD-9, LFSD-150 and variation of ripple depending on load in case of 410V input voltage.

TABLE I
POWER QUALITY RESULTS FOR VARYING LOAD CONDITION

LFSD-9	LFSD-150	Ripple	Load (W)	Voltage (V)
7E-15	7E-15	1E-15	0	410
0.79	0.79	6E-5	100	410
0.49	0.49	1E-5	280	410
0.82	0.82	9E-5	1500	410
0.83	0.83	1E-4	2900	410
0.69	0.69	0.03	5000	410

The following figures are obtained in the case of 5kW load condition.

Fig. 7 shows APD variation under varying input voltage. As seen in Fig. 7, the variation of APD decrease with the voltage. Adversely, as illustrated in Fig. 8, CE variation rises with input voltage.

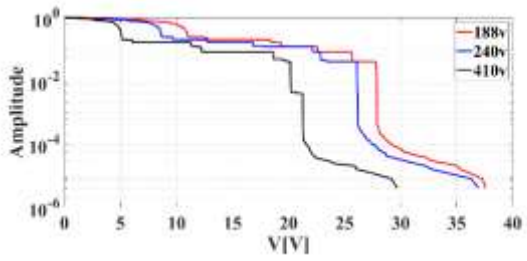

Figure 7. 5-10msec window length, variation of APD depending on input voltage at 5000W load

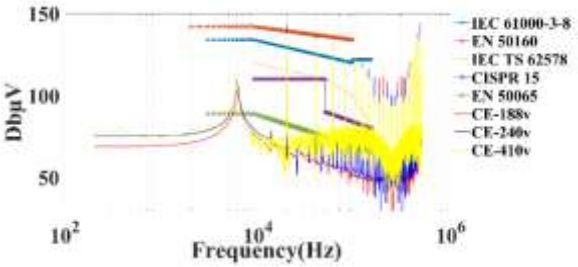

Figure 8. 5-10msec window length, variation of transmitted emissions depending on input voltage at 5kW load

Table 2. Variation of LFSD-9, LFSD-150 and ripple depending on load in case of different input voltage in case of 5-10msec window interval and 5kW load.

TABLE II
POWER QUALITY RESULTS FOR VARYING SUPPLY CONDITION

LFSD-9	LFSD-150	Ripple	Load (W)	Voltage (V)
0.69	0.69	0.12	5000	188
0.86	0.87	0.08	5000	240
0.69	0.69	0.03	5000	410

5. SPECTOGRAM

The spectrogram generates a feature vector that shows the energy change of the harmonic in the frequency bands over time and allows you to see where the major signal energy is focused. Fig. 9 depicts the spectrogram of the STFT-based signal. The use of a spectrogram is necessary since it was unclear if a 6 kHz harmonic signal is transient or not. According to the result, the harmonic can be observed only at the first energizing moment and not at subsequent sampling times. Depending on the switching frequency, harmonics of 20kHz and their multiples are observed during switching frequency.

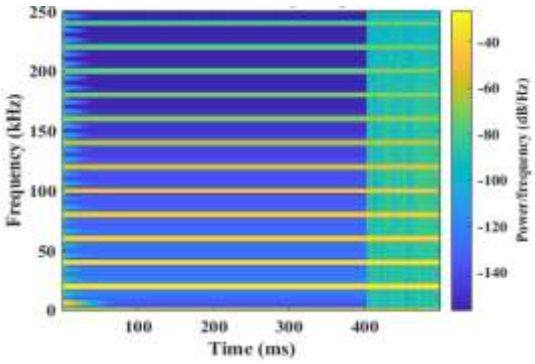

Figure 9. Spectrogram of EMI signals

6. WAVELET ANALYSIS

6.1. Discrete wavelet transform

Because STFT has a fixed frequency resolution, it poses problems. A wide window improves frequency resolution but degrades temporal resolution. A small window provides excellent temporal resolution but poor frequency resolution. These are known as narrow-gap transformations and wide-range transformations, respectively. Wavelet packet decomposition of the digitized signal is an alternative to the STFT-based technique. Instead of a discrete number of frequency components as in the Fourier transform, the wavelet transform separates the signal into numerous frequency ranges.

Figure 10 shows the discrete wavelet transform. Because the sampling frequency is 500kHz and the upper frequency is 250kHz due to the Nyquist theorem, the high and low frequency components are shown in Fig. 13. Normally, this iterative procedure is repeated until the number of samples remains constant. The application's criterion is based on achieving the best answer with the aid of 'entropy.'

$$k = \log_2 N \tag{8}$$

where N is the number of sampled signals and k is the resolution level. Since each window contains 2500 samples, the resolution level that may be reduced, k, is determined to be 11. When the 11th level of Mallat's wavelet tree (Fig. 13) is inspected, it offers the resolution of frequencies less than 50 Hz. Table 3 shows MDL findings for the sampled signal at 5-10 ms time intervals with an input voltage of 410V and a load of 1500W. When wavelet families were evaluated within themselves, the most suitable families were determined to be db20 from the Daubechies family, sym3 from the Symlets family, coif2 from the Coiflet family, bior5.5 from the biorthogonal family, reverse biortogonal rbio2.6, dmey from the discrete Meyer family, and fk22 from the Fejér-Korovkin filter family. Among the wavelet families, db20 with the lowest MDL was picked as the best fit.

TABLE III
VARIATION OF RIPPLE DEPENDING ON DIFFERENT WINDOW STATES IN CASE OF 410 V INPUT VOLTAGE

Filter	MDL	Filter	MDL	Filter	MDL	Filter	MDL
db1	52.8	sym2	49.6	coif1	51.6	rbio1.1	52.8
db2	49.6	**sym3**	**47.5**	**coif2**	**51.1**	rbio1.3	53.8
db3	47.5	sym4	48.9	coif3	50.8	rbio1.5	52.8
db4	48.2	sym5	50.9	coif4	50.5	rbio2.4	49.7
db5	46.4	sym6	50	coif5	50.3	**rbio2.6**	**48.7**
db6	44.5	sym7	52.5	bior1.1	52.8	rbio2.8	49.762
db7	44.8	sym8	49.1	bior1.3	52.1	rbio3.3	45.2
db8	44.5	sym9	50.3	bior1.5	50.6	rbio3.5	44.1
db9	42.5	sym10	49.8	bior2.4	55.6	rbio3.7	45.2
db10	42.3	sym11	49.3	bior2.6	53.9	rbio3.9	44.1
db11	43.2	sym12	49.4	bior2.8	54.2	rbio4.4	50.9
db12	40.9	sym13	49	bior3.3	59	rbio5.5	50.5
db13	40.7	sym14	50	bior 3.5	56.1	rbio6.8	51.1
db14	41.9	sym15	50.2	bior3.7	55.7	dmey	49.8
db15	39.2	sym16	48.8	bior4.4	54.3	fk4	53.5
db16	39.8	sym17	49.8	**bior5.5**	**50.2**	fk6	48.04
db17	40.2	sym18	50.1	bior6.8	52.7	fk8	48.05
db18	37.9	sym19	50.7			fk14	47.2
db19	38.2	sym20	48.5			**fk22**	**44.7**
db20	**38.1**						

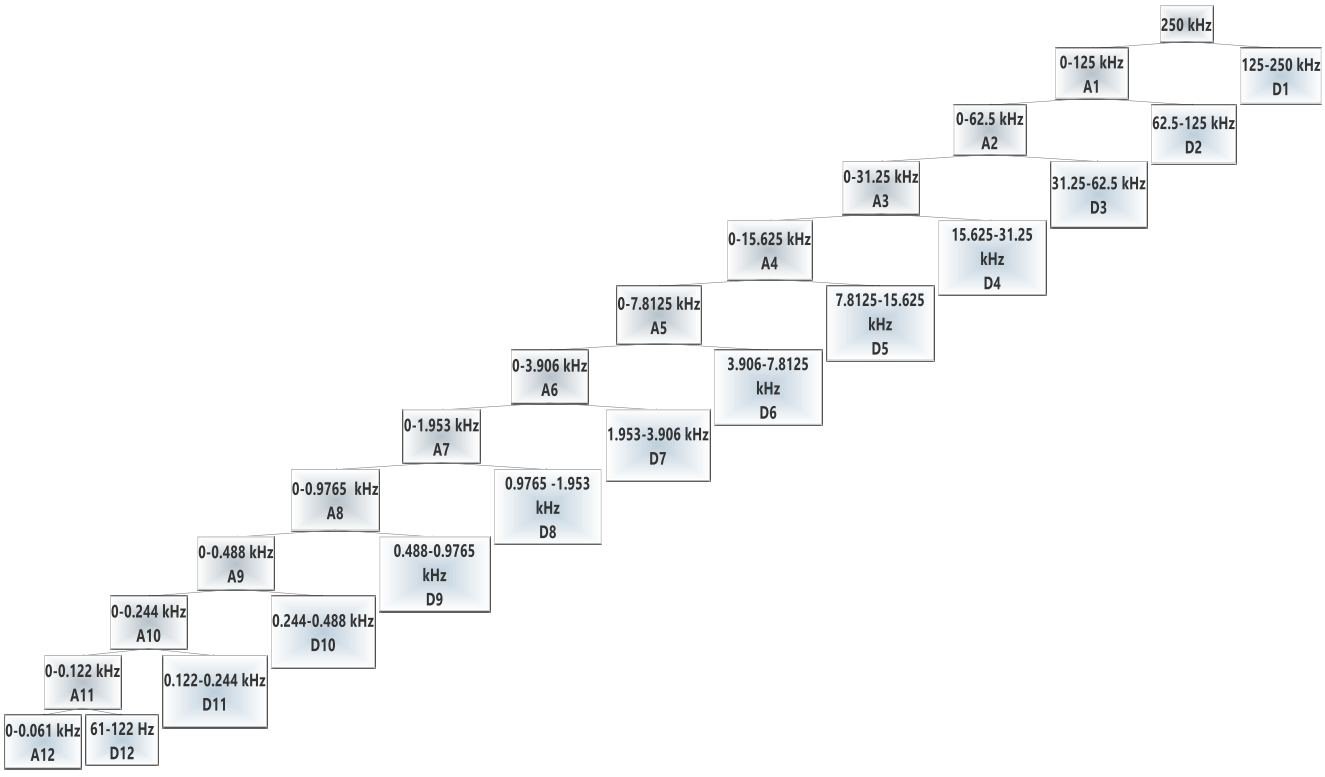

Figure 10. Approximation and detail coefficients of the analyzed signal and their frequency ranges

The appropriate decomposition level of the multiple resolution analysis was determined using Shannon entropy. This function computes the entropy of each resolution level. The level is determined by the point at which the approach and detail coefficients reverse direction. When the entropy curve in Fig. 11 is inspected, the approximation and detail coefficients for db20 change direction at the fourth level. Because we want to observe 50Hz in our research and our data load is not too high, we will need to go down to the 4th level for data load applications. As a result, it was requested to descend to the 11th floor and observe the 50Hz indicator.

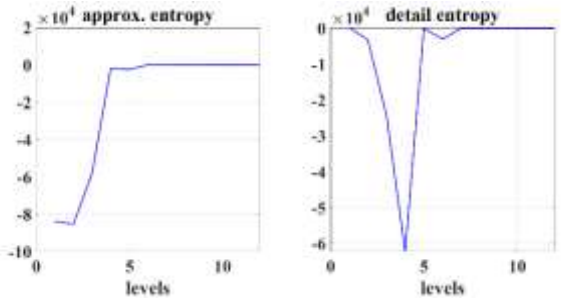

Figure 11. Calculation of the optimal decomposition level of Db20 wavelet families

Fig. 12 shows the energy levels of approximation and detail coefficients depend on db20 wavelet family.

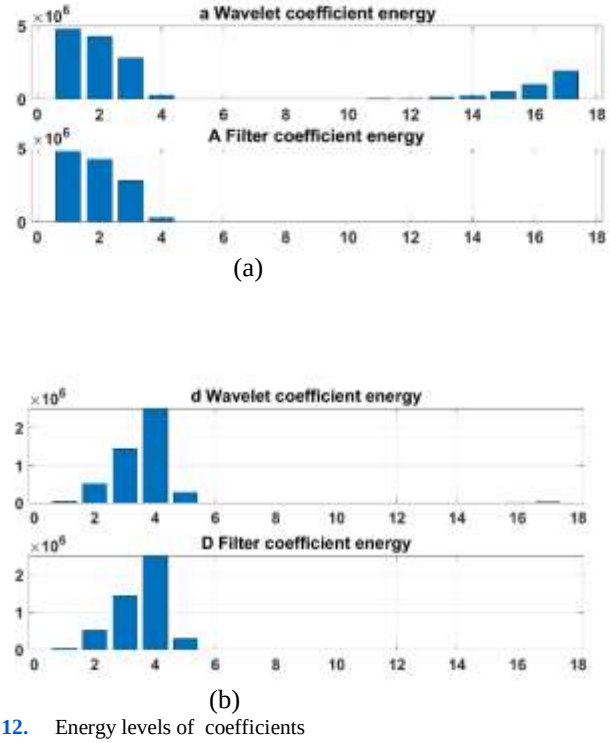

Figure 12. Energy levels of coefficients

The energy of the d wavelet coefficients suited for high frequency analysis is crucial in this study. When the energy of the d coefficients shown in Fig. 12 (b) is analysed, the d4 wavelet encompassing 20 kHz, which is the switching frequency, has the maximum energy. The switching signal d3 at 40kHz corresponds to the frequency range covered by the wavelet coefficient, 60kHz to the range covered by d2, and 6kHz to the range covered by d5 and d6. Because d5 has a larger frequency range, its energy stays greater than d6. Because the LISN device did not pass the 50 Hz low frequency signal, the d11 energy was insufficient

When using the 'multiresolution analyzer' toolbar from MATLAB™ tools. The energy of the signal obtained in wavelet transform 4th level analysis is approximately half of the energy of the whole signal. The influence of the filter coefficients will be especially important in filter designs to reduce harmful interference of EMI signals.

6.2. Multi-resolution analysis

The wavelet packet spectrum comprises the absolute values of the coefficients from the binary wavelet packet tree's frequency sorted end nodes. In wavelet packet transform, terminal nodes give the highest level of frequency resolution. J denotes the wavelet packet transformation level, while Fs is the sampling frequency. Equation 9 is used to compute the width of the band to the end nodes. The wavelet packet spectrum comprises the absolute values of the coefficients from the binary wavelet packet tree's frequency sorted end nodes. In wavelet packet transform, terminal nodes give the highest level of frequency resolution. J denotes the wavelet packet transformation level, while Fs is the sampling frequency. The width of the band to the end nodes is calculated by equation 9 [23].

$$\left[\frac{nFs}{2^{j+1}}, \frac{(n+1)Fs}{2^{j+1}}\right] \quad n = 0,1,2,3,\dots 2^{j} - 1 \tag{9}$$

Fig. 13 shows an example of a 2nd level wavelet tree structure in which the same logic decomposes at further levels to make the wavelet packet tree more accessible.

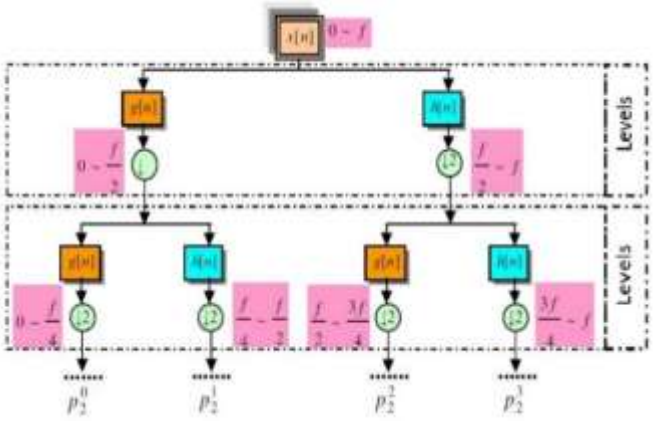

Figure 13. Energy change of the harmonic in the relevant frequency range according to the resolution level

Fig. 13 shows 2nd level multi-resolution analysis and its associated frequency ranges. Suppose that x(t) signal has N = 2^L samples and decomposed up to s. level packet analysis. In this case, here will be 2^s nodes/packets or frequency bands, and there are $2^{(L-s)}$ or N / 2^s wavelet packet coefficients in each level band. For m=0,1…..,2^s-1, wavelet packet coefficients of m node and k level is expressed as $p_s^{2m}[k]$ and calculated as follow:

$$X_{RMS}^{m} = \sqrt{\frac{1}{N}\sum_{k=1}^{N/2^s}\{p_s^m[k]\}^2} \tag{10}$$

When the wavelet tree analysis is done using the db20 family, which was chosen based on the Shannon entropy result, the effective value of the wavelet coefficients of each node is

determined using equation 10. Analysis up to level 6 is necessary to meet the frequency range criteria (above 2kHz). However, in the sixth level, the switching frequency corresponds to a signal with a frequency range of 27.344 - 31.250kHz and the greatest amplitude given in Fig. 14. The switching frequency is more readily noticed at the 11th level for the comparative assessment of wavelet packet analysis with STFT since there are nodes with a band gap of 122.0703 Hz. As a result, the switching frequency falls within the range of 29.785 - 29.907.

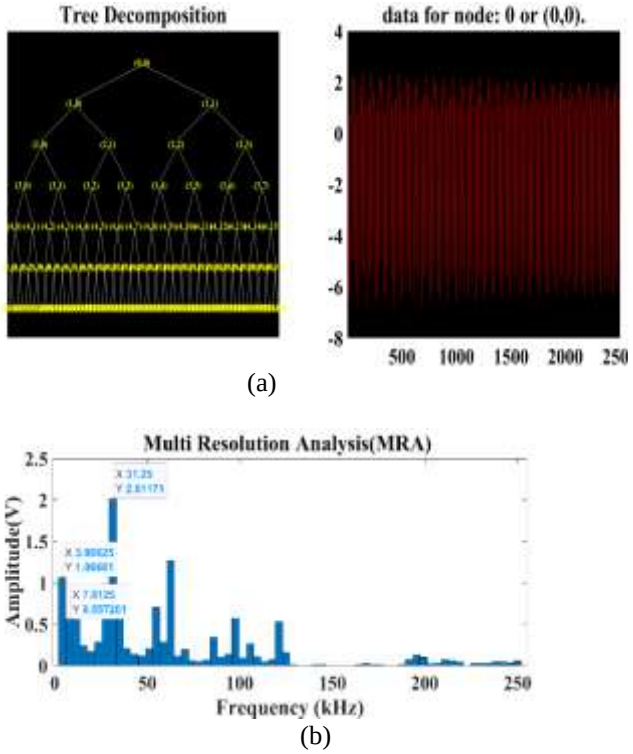

Figure 14. Energy change of the harmonic in the relevant frequency range according to the resolution level

In summary, discrete wavelet transform gives harmonics a wider band. MRA was used to harmonic analysis detailed to evaluate whether harmonic leakage exists. Wavelet analysis has performed an alternative for STFT. However, because wavelets cover a wide frequency range, they are inadequate for emissions investigation.

7. EMI FILTER for BUCK CONVERTER

It is necessary to utilize filters to reduce high-frequency noise because filters are frequently situated and created to satisfy standard criteria. Filtering makes a product less susceptible to any existing high-frequency noise in the environment while also preventing the product from causing high-frequency interference. Early design consideration of EMI could assist designers in efficiently meeting EMC regulations prior to implementation. To reduce design process and costs, EMI forecast should be properly taken care of by precise design. In this section in PSIM software environment suppression of noise was simulated and given in Fig. 17. PI controller of output voltage and LISN are seen in Fig. 15 and Fig. 16. Also, output voltage of converter is given in Fig. 18.

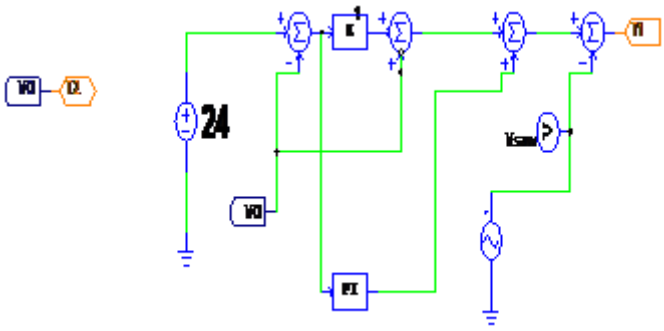

Figure 15. PI controller of buck converter

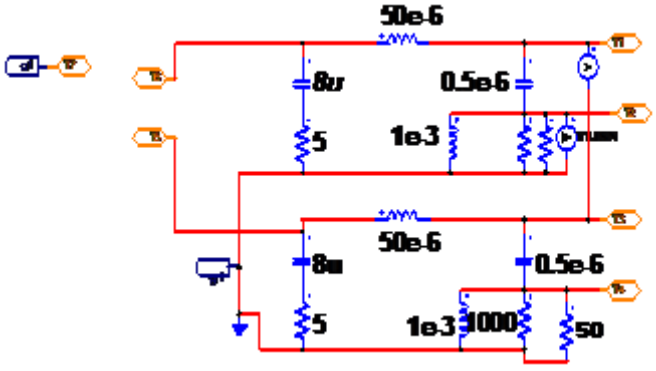

Figure 16. LISN device of buck converter

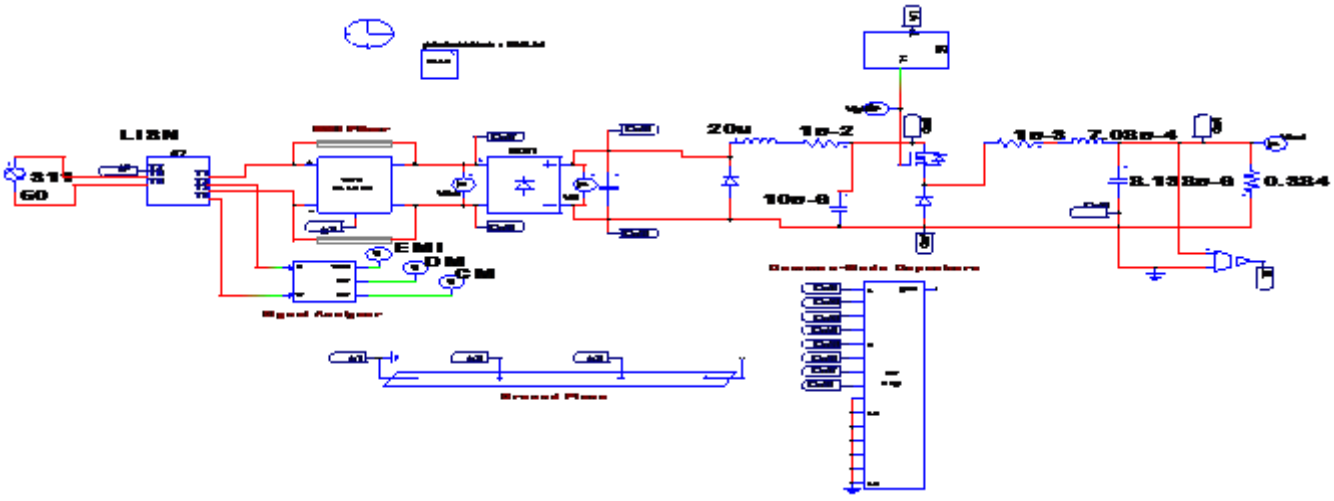

Figure 17. EMI Filter Design of Buck Converter (CISPR 22 Class-B)

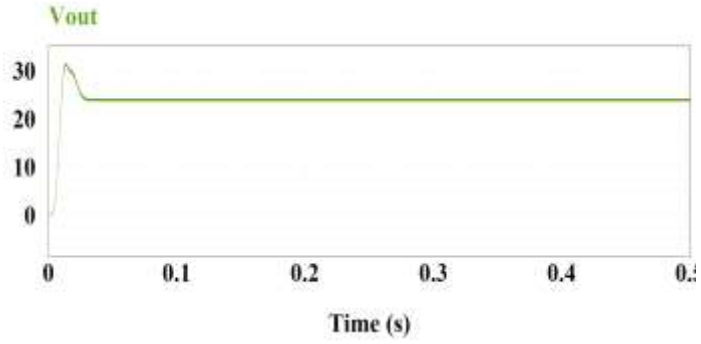

Figure 18. Output voltage of Converter

EMI, DM, and CM signals are obtained through 'signal analyzer' in the simulation and shown in Fig. 19.

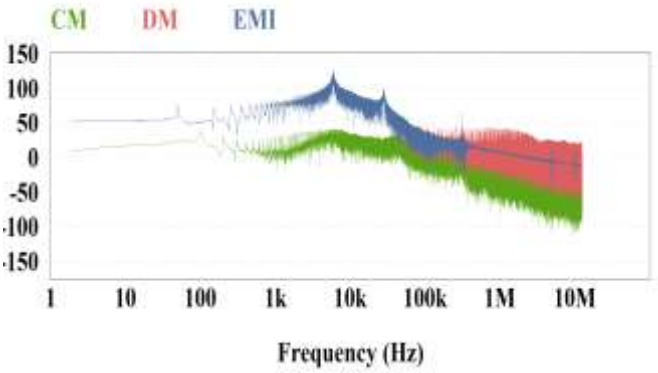

Figure 19. EMI, DM, and CM signals

For suppression of noise EMI filter parameters given in Table IV. When these filter parameters used for EMI filter, suppression of noise is supported with Fig. 20.

TABLE IV
EMI FILTER PARAMETERS

	Parameter	Value
EMI Filter	Filter enable	0
	Filter type	0
	Num. stage	1
	Cx	6.13nF
	R_Cx	0
	L_Cx	1.2µH
	Cy	2.04 nF
	R_Cy	0
	L_Cy	15.78 µH
	k_leakage_cm	0.05
	R_cm	0.1mΩ
	C_cm	0
	R_dm	0.1mΩ
	Cd	0
	R_Cd	0
Common Mode EMI	freq_cm_EMI	59.9kHz
	Amp_cm_EMI	55
	Amp_cm_EMI_Std	36.8
Differential Mode EMI	freq_dm_EMI	59.5kHz
	Amp_dm_EMI	128.6
	Amp_dm_EMI_Std	36.8
Common Mode Capacitance	Ccm1,Ccm2	500pF
	Ccm3,Ccm4, Ccm7,Ccm8	50pF
	Ccm5,Ccm6	100pF

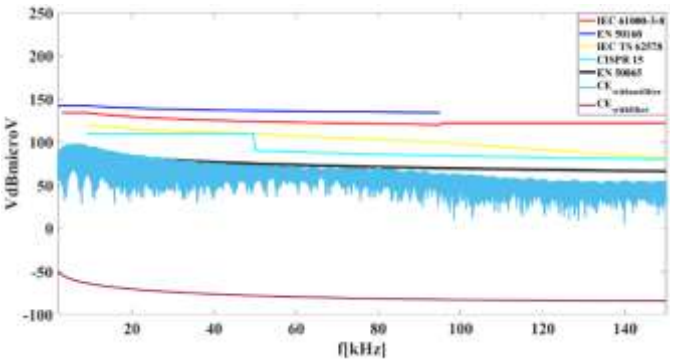

Figure 20. Suppression of noise

8. CONCLUSION

The goal of this project was to emphasize the importance of CEs, which will become more widespread as the use of electric vehicles and led driver grows in general. In this study power quality analysis of conducted emissions was performed for buck converter in MATLAB and PSIM software environments. The solution approach to reduce the power quality problem based on this converter is explained. Reducing CE with EMI filter design is difficult for power electronics applications, particularly inverters. Because a filter's design is unique to the circuit, it is necessary to construct a noise model of the circuit. In this research also, spectrum of the signals was calculated using the STFT technique in MATLAB™ tools for the evaluation of disturbances The intended result could not be attained using db20, the most appropriate wavelet family for the signal among the standard wavelet families. The EMI requirements for converters because of international standards are discussed. It has been demonstrated that conducted emissions are higher in the case of nonfilter buck converter situation. As a result, the CE attenuation was preserved this buck converter system in PSIM. Another results are summarized as below:

• Power quality evaluation of DC-DC converter performed in Matlab simulation environment in terms of emissions.

• LFSD increased in loaded condition compared to unloaded condition. Considering the last half-time of the sampling time, which is out of the transient state, generally the CE to the grid side increases depending on the load increase.

• APD and ripple index decreased as the input voltage increased.

• CE and DFSB increase as the input voltage increases.

• While the DFSB index decreases in the last window intervals of the sampled time compared to the first time intervals, the fluctuation remains constant.

• When the spectrogram of the signal (analysis that gives the energy of the frequency dependent on time) of the 6 kHz frequency other than the switching frequency in the analysis with STFT is examined, it has been observed that this frequency does not occur during the entire sampling frequency, but during the temporary period. However, in wavelet transform, both low and high frequency analysis can be performed at the same time. At the same time, the change in frequency over time can be observed. For this purpose, when the discrete wavelet transform analysis was performed first, it

was seen that the energy of the relevant frequency range and the amplitude responses of the frequencies in the STFT were compatible. In order to make a more detailed and comparison, spleen packet analysis was performed by choosing the most suitable family from the traditional wavelet family. At the same time, the amplitude of the harmonics corresponding to the frequency range at the nodes was calculated to evaluate for the standard limits. However, since the response of the harmonics is incompatible with the STFT, it was thought that the analysis with the 'Vaidyanathan filter' used in the amplitude response of the harmonics in the wavelet packet analysis would be more appropriate.

ACKNOWLEDGEMENT

This work was supported in part by Ondokuz Mayis University under Projects PYO.MUH.1904.21.011 and PYO.MUH.1906.21.002

REFERENCES

[1] D D. Ritzmann, et al.,"Comparison of measurement methods for 2–150-kHz conducted emissions in power networks", IEEE Transactions on Instrumentation and Measurement,vol 70, pp. 1-10, 2020.

[2] A. D. Khilnani, et al. "Power quality analysis (0-2kHz) in DC/DC converters under steady state and transient conditions", presented at the International Symposium on Electromagnetic Compatibility-EMC EUROPE, Amsterdam, Netherlands, Aug. 2-5,27-30 2018.

[3] K. Niewiadomski, et al., "Time-domain assessment of data transmission errors in systems with multiple DC/DC converters", presented at the 2020 International Symposium on Electromagnetic Compatibility-EMC EUROPE, Rome, Italy, Sep. 23-25, 2020.

[4] A. Onur et al., "Determination of the optimum Hybrid renewable power system: a case study of Istanbul Gedik University Gedik Vocational School", Balkan Journal of Electrical and Computer Engineering, vol. 7, no.4, pp. 456-463, 2019.

[5] E. Aykut, et al. "Techno-economic and environmental analysis of grid connected hybrid wind/photovoltaic/biomass system for Marmara University Goztepe campus", International Journal of Green Energy, vol. 17, no.15, pp. 1036-1043, 2020.

[6] L. Ensini, et al. 2018. "Conducted emissions on DC power grids", presented at the 2018 International Symposium on Electromagnetic Compatibility (EMC EUROPE), Amsterdam, Netherlands, Aug, 27-30, 2018.

[7] D. Kumar, et al., "DC microgrid technology: system architectures, AC grid interfaces, grounding schemes, power quality, communication networks, applications, and standardizations aspects", IEEE Access, vol. 5, pp. 12230-12256,2017.

[8] F. Leferink, "Conducted interference, challenges and interference cases", IEEE Electromagnetic Compatibility Magazine, vol. 4, no. 1, pp. 78-85, 2015.

[9] A. Mariscotti, "Discussion of power quality metrics suitable for DC power distribution and smart grids", presented at the Proc. 24th IMEKO TC4 Int. Symp, Sep. 17-20, Xi'an, China, 2019.

[10] M., Miloudi, et al.,"Common and differential modes of conducted electromagnetic interference in switching power converters", Rev. Roum. des Sci. Tech. Ser. Electrotech. Energ., vol. 62, no. 3, pp. 246–251, 2017.

[11] S. Weßling and S. Dickmann, "Prediction of conducted emissions produced by a DC-DC-converter using component parasitics and partial inductances", presented at the 2013 International Symposium on Electromagnetic Compatibility, Brugge, Belgium, Sep. 2-6,2017.

[12] E.A. Larsson, et al., "Measurements of high-frequency (2–150 kHz) distortion in low-voltage networks", IEEE Transactions on Power Delivery, vol. 25, no. 3, pp. 1749-1757, 2010

[13] F. Krug and P. Russer, "Quasi-peak detector model for a time-domain measurement system." IEEE Transactions on Electromagnetic Compatibility, vol. 47, no.2, pp. 320-326, 2005.

[14] G. Spadacini, et al., "Conducted emissions in the powertrain of electric vehicles", presented at the 2017 IEEE International Symposium on Electromagnetic Compatibility & Signal/Power Integrity (EMCSI), Washington, DC, USA, Aug 7-11, 2017.

[15] G. Spadacini, et al., "SPICE simulation in time-domain of the CISPR 25 test setup for conducted emissions in electric vehicles", presented at the 2015 Asia-Pacific Symposium on Electromagnetic Compatibility (APEMC), Taipei, Taiwan, May 26-29, 2015.

[16] A. Larrson, and M. Bollen “A proposal for emission and immunity of equipment including power-line communication.” [Online]. Available: https://www.arbenelux.com/wp-content/uploads/2017/11/Tekbox-TBOH01-LISN.pdf. [Accessed: 7-Dec-2022].

[17] N. Mutoh, et al., "Control methods for EMI noises appearing in electric vehicle drive systems", presented at the Twentieth Annual IEEE Applied Power Electronics Conference and Exposition, Austin, TX, USA, Mar, 6-10, 2015.

[18] H. Shall and M. Kadi, "Study of the radiated emissions of an electric vehicle battery charger during the charge cycle", presented at the 2015 IEEE 12th International Multi-Conference on Systems, Signals & Devices (SSD15), Mahdia, Tunisia,Mar 16-19,2015.

[19] P.K.P. Ferraz, et al., "A high frequency model for predicting the behavior of lithium-ion batteries connected to fast switching power electronics", Journal of Energy Storage, vol. 18, pp. 40-49,2018.

[20] T. Karaca, et al., "EMI-receiver simulation model with quasi-peak detector", 2015 IEEE International Symposium on Electromagnetic Compatibility, Dresden, Germany, Aug 16-22, 2015.

[21] T. Sonmezocak et al., "High performance adaptive high performance adaptive active harmonic filter design for nonlinear led loads", Light & Engineering, vol. 30, no.1, 2022.

[22] S. Dursun, et al., "Comparative analysis of lighting elements’ effects on electric system", European Journal of Technique (EJT), vol. 11, no. 2, pp. 153-164, 2021.

[23] V. Fahri, "RMS and power measurement using the dual-tree complex wavelet transform", Scientific Research and Essays, vol. 5, no. 18 pp. 2645-2655, 2010.

BIOGRAPHIES

Secil GENC was born in Elazıg in 1992. She received her B.Sc degree from Firat University in 2014 and M.Sc. degree from Ondokuz Mayis University in 2018. She is currently pursuing Ph.D. degree in Electrical and Electronics Engineering Department at Ondokuz Mayis University, Samsun, Turkiye. She is also a research assistant at Ondokuz Mayis University. Her research interests include power electronics, electromagnetic interference, renewables and machine learning.

Okan OZGONENEL was born in Samsun in 1967. He worked for Goztepe SSK Hospital as an engineer from 1989 to 1991. Then he received a special grant and promoted as Lecturer in Amasya Technical and Vocational Higher School by means of World Bank Second Industrial Training Project. He has worked there for 10 years and then joined Ondokuz Mayis University, Electrical & Electronic Engineering Department in 2002. He was promoted as full Professor in 2014 and since then he has been working for Ondokuz Mayis University where he is full time Professor. He joined The University of Nottingham many times for his post-doctoral studies.
His main research includes power system modeling, protection, and renewables.

Orkut Onat YILDIZ graduated from Karadeniz Technical University's Electrical Department in 2002 and He graduated from Anadolu University's Faculty of Economics in 2019. He worked as a laboratory supervisor at Borsan Kablo from 2006 to 2010, as a Quality Manager from 2010 to 2018, and as an R&D manager since 2019.

İbrahim Hakkı KILIÇ received his bachelor's degree in Materials Science and Ceramics Engineering from Dumlupnar University in 2011, and he is currently pursuing my master's degree in the Textile Engineering Department at Istanbul Technical University. He worked as a production manager at Işıldar Aydınlatma between 2013 and 2017, and as of 2019, He worked as a lighting group R&D and quality manager at Borsan Kablo ve Lighting. His specialties include 3D modeling and automation systems.
.